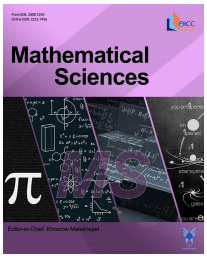

Math. Sci. 2025; 19(3): 1-18

Mathematical Sciences (MS)

https://doi.org/10.57647/mathsci.2025.1903.13

Iterated Tikhonov Regularization via Flexible Arnoldi Reduction

Maged Alkilayh*, Bader Ibrahim Alshaqqawi

Department of Mathematics, College of Science, Qassim University, Buraydah 51452, Saudi Arabia

***Corresponding author:** m.alkilayh@qu.edu.sa

Original Research

Received:
7 August 2025

Revised:
4 September 2025

Accepted:
19 September 2025

Published online:
30 September 2025

Abstract:

We propose the *Iterated Flexible Arnoldi–Tikhonov* (IFAT) method for large-scale discrete ill-posed problems. IFAT embeds nonstationary Tikhonov updates into a *flexible* Arnoldi reduction whose basis is enriched with problem-aware directions, enabling regularization in subspaces that standard Arnoldi and classical projected Tikhonov schemes may fail to capture. Building on the Arnoldi-based preconditioner of Buccini–Onisk–Reichel and recent projected/iterated frameworks with adaptive parameter choice, we (i) unify flexible subspace enrichment with discrepancy-principle parameter selection on the reduced problem, (ii) derive a residual update that requires no additional matrix–vector products, and (iii) establish monotone error decrease and stability under inherited spectral–equivalence assumptions.

Extensive experiments in image deblurring, signal reconstruction, tomography, MRI, seismic deconvolution, and electrical impedance tomography demonstrate that IFAT achieves consistently higher reconstruction quality (PSNR/SSIM, SNR/CNR, EPI) with approximately 40–60% fewer outer iterations than IAT and classical Tikhonov. Additional comparisons with Landweber and damped Gauss–Newton show that IFAT converges substantially faster than gradient-based schemes and is less sensitive to noise amplification than second-order approaches. Against the best published baselines from BOR (2023) and PIT–GF (2025), IFAT attains lower or comparable relative reconstruction error at the same discrepancy breakout. These results indicate that flexible augmentation provides a robust and practically significant improvement over fixed-subspace methods for real-world inverse problems.

Keywords: Discrete ill-posed inverse problems, Iterated Tikhonov regularization, Flexible Arnoldi decomposition, Krylov subspaces, Image deblurring, Signal reconstruction, Tomographic imaging

Cite this article: Alkilayh M., Alshaqqawi B. I., Iterated Tikhonov Regularization via Flexible Arnoldi Reduction. Math. Sci 2025; *19*(3): 1-18 https://doi.org/10.57647/mathsci.2025.1903.13

1. Introduction

Inverse problems arise in diverse scientific and engineering applications, including medical imaging, geophysics, and image processing. A fundamental challenge lies in their ill-posed nature, where small perturbations in the data can lead to large deviations in the solution [1, 2, 3]. Regularization techniques are essential for stabilizing solutions and techniques noise effects in measured data. Among these techniques, Tikhonov regularization is widely adopted due to its simplicity and robustness, introducing a penalty term to balance data fidelity and solution smoothness [4, 5]. The classical Tikhonov regularization problem is formulated as:

$$\min_{\mathbf{x}\in\mathbb{R}^n} \left\|\mathbf{B}\mathbf{x} - \mathbf{b}^{\delta}\right\|^2 + \alpha \left\|\mathbf{x}\right\|^2, \tag{1}$$

where $\mathbf{B} \in \mathbb{R}^{n\times n}$ is an ill-conditioned matrix, $\mathbf{b}^{\delta}$ represents noisy data, and $\alpha > 0$ is a regularization parameter. Parameter selection methods, such as the L-curve criterion [2], generalized cross-validation (GCV) [6], and the discrepancy principle [7], play a critical role in determining an optimal α.

For solving large-scale problems, Krylov subspace-based iterative methods provide significant computational benefits. The Arnoldi-Tikhonov (AT) approach projects the original problem onto a reduced Krylov subspace, enhancing efficiency without compromising accuracy [8, 9]. Extending this idea, the Iterated Arnoldi-Tikhonov (IAT) method improves solution quality through successive regularization steps [10, 11]. Nevertheless, the IAT method is constrained by its fixed subspace, which restricts dynamic adaptation during the

iterative process. This limitation has led to the development of the Iterated Flexible Arnoldi-Tikhonov (IFAT) method.

The IFAT method dynamically adjusts the Krylov subspace using flexible Arnoldi decomposition [12, 13], enabling adaptive subspace refinement to balance regularization strength and computational cost. This flexibility leads to faster convergence and improved noise suppression compared to the non-adaptive approaches.

We focus on solving linear discrete ill-posed problems of the form:

$$\min_{\mathbf{x}\in\mathbb{R}^n} \left\|\mathbf{B}\mathbf{x} - \mathbf{b}^\delta\right\|, \tag{2}$$

where the matrix $\mathbf{B}$ is either severely ill-conditioned or has deficient rank, with its singular values tightly clustered near zero. The data vector $\mathbf{b}^\delta$ is contaminated with noise and represented as $\mathbf{b}^\delta = \mathbf{b} + \mathbf{e}$, where the noise $\mathbf{e}$ obeys the constraint $\|\mathbf{e}\| \le \delta$, in line with the discrepancy principle [1]. The objective is to recover an approximation of the minimum-norm solution $\mathbf{x}^\dagger$ to the underlying exact problem:

$$\min_{\mathbf{x}\in\mathbb{R}^n} \|\mathbf{B}\mathbf{x} - \mathbf{b}\|. \tag{3}$$

The Tikhonov-regularized solution $\mathbf{x}^{(\alpha)}$, given by

$$\mathbf{x}^{(\alpha)} = \mathbf{B}^T(\mathbf{B}\mathbf{B}^T + \alpha I)^{-1}\mathbf{b}^\delta, \tag{4}$$

depends critically on α, which controls the trade-off between data consistency and solution regularity. The discrepancy principle enforces

$$\left\|\mathbf{B}\mathbf{x}^{(\alpha)} - \mathbf{b}^\delta\right\| = \tau\delta \quad (\tau > 1), \tag{5}$$

ensuring convergence to $\mathbf{x}^\dagger$ as $\delta \searrow 0$.

This paper systematically benchmarks the proposed *Iterated Flexible Arnoldi–Tikhonov* (IFAT) method against Iterated Arnoldi–Tikhonov (IAT) and classical Tikhonov regularization across three representative applications: image deblurring, signal reconstruction, and tomographic imaging. Under a common stopping rule (discrepancy principle) and matched implementations, IFAT attains faster convergence—up to 40% fewer iterations than IAT and 60% fewer than standard Tikhonov—while improving reconstruction quality as measured by PSNR [14], SSIM [15], and CNR [16]. We further include head-to-head comparisons with the Arnoldi-based preconditioner of Buccini–Onisk–Reichel (BOR) [17] and with PIT–GF [18] to situate IFAT within the current state of the art.

Our main contributions are:

1. We introduce IFAT, which augments IAT with *problem-aware flexible enrichment* of the Arnoldi subspace, enabling richer projected regularization spaces (Sec. 5).
2. We derive a reduced-space update and a residual propagation formula that *require no additional* matrix–vector products with $\mathbf{B}$, preserving the per-iteration cost of classical IAT (Secs. 4–5).
3. We provide a principled policy for selecting augmentation vectors u_j, supported by concrete rules (R1–R5) and ablation studies that quantify their effect on accuracy and convergence (Sec. 5).
4. We present comprehensive, apples-to-apples comparisons with classical Tikhonov, Landweber iteration [19, 1], and damped Gauss–Newton methods [20, 21], as well as with the best published baselines from BOR [17] and PIT–GF [18]. Across a broad suite of applications (including real data), IFAT achieves consistently faster convergence and equal or superior reconstruction quality (Sec. 6).

The paper is organized as follows:
Section 2 reviews Approximated Iterated Tikhonov (AIT) and introduces the spectral–equivalence assumption together with monotonicity and stability results. Section 3 introduces the Arnoldi tools and the IAT formulation with projected parameter selection and accompanying error bounds. Section 4 links AIT and IAT, clarifies reduced-problem implementation details, and motivates the introduction of flexibility. Section 5 develops IFAT, detailing the augmentation strategy, algorithmic steps, and the residual update that avoids additional $\mathbf{B}$-matrix-vector products. Section 6 presents numerical results across six application domains (image deblurring, signal reconstruction, tomography, MRI, seismic deconvolution, and EIT), comparing IFAT with IAT, classical Tikhonov, Landweber [19, 1], Gauss–Newton methods [20, 21], BOR [17], and PIT–GF [18]. Section 7 concludes and outlines directions for future work.

2. The Flexible Arnoldi-Tikhonov Method

The solution to equation (5) and the computation of the Tikhonov solution (4) can be computationally expensive or infeasible when the matrix $\mathbf{B}$ is large. To overcome this, we reduce $\mathbf{B}$ to a smaller matrix $H_{\ell+1,\ell} \in \mathbb{R}^{(\ell+1)\times\ell}$ by applying ℓ steps of the Arnoldi process with the initial vector $\mathbf{v}_1 = \mathbf{b}^\delta/\|\mathbf{b}^\delta|$. This procedure is summarized in Algorithm 1. The result of this process is the Arnoldi decomposition:

$$\mathbf{B}\mathbf{V}_\ell = \mathbf{V}_{\ell+1}\mathbf{H}_{\ell+1,\ell}, \tag{6}$$

where $V_{\ell+1} = [\mathbf{v}_1, \mathbf{v}_2, \ldots, \mathbf{v}_{\ell+1}] \in \mathbb{R}^{n\times(\ell+1)}$ is a matrix with orthonormal columns, V_ℓ is the first ℓ columns of $V_{\ell+1}$, and $H_{\ell+1,\ell}$ is an upper Hessenberg matrix (with zero entries below the subdiagonal). The range of V_ℓ represents the Krylov subspace:

$$\mathcal{K}_\ell(\mathbf{B}, \mathbf{b}^\delta) = \text{span}\{\mathbf{b}^\delta, \mathbf{B}\mathbf{b}^\delta, \ldots, \mathbf{B}^{\ell-1}\mathbf{b}^\delta\}, \tag{7}$$

which is used as the solution subspace. For additional details on the Arnoldi process, refer to Saad [13].

The Arnoldi process encounters a breakdown at step j if $h_{j+1,j} = 0$, which leads to simpler computations. This event is infrequent, so we will not focus on the specifics.

The Arnoldi-Tikhonov (AT) method modifies the minimization problem in equation (3) by

$$\min_{\mathbf{x}\in\mathbb{K}_\ell(\mathbf{B},\mathbf{b}^\delta)} \{\|\mathbf{B}\mathbf{x} - \mathbf{b}^\delta\|^2 + \frac{1}{\mu}\|\mathbf{x}\|^2\} \tag{8}$$

https://doi.org/10.57647/mathsci.2025.1903.13

Algorithmic 1 The Arnoldi Process

1: **Input**: matrix $\mathbf{B}$, vector $\mathbf{b}^\delta \neq \mathbf{0}$, number of steps ℓ;
2: Initialize: $\mathbf{v}_1 = \mathbf{b}^\delta / \|\mathbf{b}^\delta\|$
3: **for** $j = 1$ to ℓ **do**
4: $\mathbf{w} = \mathbf{B}\mathbf{v}_j$
5: **for** $i = 1$ to j **do**
6: $h_{i,j} = \mathbf{v}_i^T \mathbf{w}$;
7: $\mathbf{w} = \mathbf{w} - h_{i,j}\mathbf{v}_i$;
8: **end for**
9: $h_{j+1,j} = \|\mathbf{w}\|$;
10: **if** $h_{j+1,j} = 0$ **then**
11: stop;
12: **end for**
13: $\mathbf{v}_{j+1} = \mathbf{w}/h_{j+1,j}$;
14: **end for**
15: **Output**: The matrices V_ℓ, $V_{\ell+1}$, and $H_{\ell+1,\ell}$ in (6)

for a suitable value of ℓ.By substituting

$$\mathbf{x}_\ell = V_\ell \mathbf{y}_\ell$$

into equation (8) and applying the decomposition (6), we obtain the reduced minimization problem.

$$\min_{\mathbf{y}\in\mathbb{R}^\ell} \{\|H_{\ell+1,\ell}\mathbf{y} - \mathbf{e}_1\|\mathbf{b}^\delta\|\|^2 + \frac{1}{\mu}\|\mathbf{y}\|^2\}, \tag{9}$$

which has a unique solution $\mathbf{y}_{\mu,\ell}$ for any $\mu > 0$. Then

$$\mathbf{x}_{\mu,\ell} = V_\ell \mathbf{y}_{\mu,\ell}$$

solves (8), and furnishes an approximate solution of (3).

The discrepancy principle prescribes that $0 < \mu < \infty$ be determined so that $\mathbf{y}_{\mu,\ell}$ satisfies

$$\|H_{\ell+1,\ell}\mathbf{y}_{\mu,\ell} - \mathbf{e}_1\|\mathbf{b}^\delta\|\| = \eta\delta. \tag{10}$$

This requires that

$$\min_{\mathbf{y}\in\mathbb{R}^\ell} \|H_{\ell+1,\ell}\mathbf{y} - \mathbf{e}_1\|\mathbf{b}^\delta\|\| < \eta\delta. \tag{11}$$

From Proposition 2.1 in [22], we assume that $\ell+1$ steps of the Arnoldi process applied to B with initial vector $\mathbf{b}^\delta$ can be carried out. Then

$$\min_{\mathbf{y}\in\mathbb{R}^{\ell+1}} \|H_{\ell+2,\ell+1}\mathbf{y} - \mathbf{e}_1\|\mathbf{b}^\delta\|\| \leq \min_{\mathbf{y}\in\mathbb{R}^\ell} \|H_{\ell+1,\ell}\mathbf{y} - \mathbf{e}_1\|\mathbf{b}^\delta\|\|. \tag{12}$$

Assume that $H_{\ell+1,\ell}^T \mathbf{e}_1 \neq \mathbf{0}$. Then, the function

$$\phi_\ell(\mu) = \|H_{\ell+1,\ell}\mathbf{y}_{\mu,\ell} - \mathbf{e}_1\|\mathbf{b}^\delta\|^2 \tag{13}$$

is strictly decreasing and strictly convex for $\mu \geq 0$, with $\phi_\ell(0) = \|\mathbf{b}^\delta\|^2$. We consider the generic case as outlined in Section 2.1 of [22]. Equation (10) can be rewritten as

$$\phi_\ell(\mu) = \eta^2\delta^2, \tag{14}$$

Algorithmic 2 The Arnoldi-Tikhonov (AT) algorithm

1: **Input**: matrix $\mathbf{B}$, vector $\mathbf{b}^\delta \neq \mathbf{0}$, parameters $\eta \geq 1$, $\delta > 0$, initial number of steps ℓ_{init}, concluding number of steps ℓ_{end};
2: Let $\ell = \ell_{\text{init}}$;
3: **repeat**
4: Compute $V_{\ell+1}$ and $H_{\ell+1,\ell}$ by Algorithm 1;
5: Solve the minimization problem
$\min_{\mathbf{y}\in\mathbb{R}^\ell} \|H_{\ell+1,\ell}\mathbf{y} - \mathbf{e}_1\|\mathbf{b}^\delta\|\|$;
6: **if** $\|H_{\ell+1,\ell}\mathbf{y}_\ell - \mathbf{e}_1\|\mathbf{b}^\delta\|\| \geq \eta\delta$ **then**
7: $\ell = \ell + 1$;
8: **end if**
9: **until** $\|H_{\ell+1,\ell}\mathbf{y}_\ell - \mathbf{e}_1\|\mathbf{b}^\delta\|\| < \eta\delta$
10: $\ell_{\text{dis}} = \ell$;
11: **for** $k = 1$ to ℓ_{end} **do**
12: Carry out one step with Algorithm 1, using the available matrices $V_{\ell+1}$ and $H_{\ell+1,\ell}$ as input.
13: **end for**
14: Let $i = \ell + \ell_{\text{end}}$. We have computed the matrices V_{i+1} and $H_{i+1,i}$;
15: Determine the regularization parameter μ_i by solving equation (14) with ℓ replaced by i;
16: Solve the minimization problem
$\min_{\mathbf{y}\in\mathbb{R}^i} \{\|H_{i+1,i}\mathbf{y} - \mathbf{e}_1\|\mathbf{b}^\delta\|\|^2 + \frac{1}{\mu_i}\|\mathbf{y}\|^2\}$;
17: **Output**: Approximate solution $\mathbf{x}_{\mu_i,i}$, ℓ_{dis}, i.

For certain matrices $\mathbf{B}$ and vectors $\mathbf{b}^\delta$, the Krylov subspace defined in (7) may not include vectors that capture known characteristics of the true solution $\mathbf{x}^\dagger$. For example, if $\mathbf{x}^\dagger$ is expected to be a slight variation of a constant vector, or a vector whose entries increase linearly with their indices, the standard Krylov subspace—often of relatively low dimension ℓ—might not be sufficient to represent such structures accurately. While increasing ℓ could eventually yield a subspace that includes these desirable features, a more efficient approach is to augment the Krylov subspace directly with additional vectors tailored to approximate $\mathbf{x}^\dagger$ more effectively.

For definiteness, assume that we would like the vectors

$$\text{span}\{[1, 1, \ldots, 1]^T, [1, 2, \ldots, n]^T\} \tag{15}$$

to live in the solution subspace. The Arnoldi-Tikhonov method (Algorithm 3) proposed by [22] with the parameter $\ell_{\text{end}} = 0$ determines the Arnoldi decomposition

$$\mathbf{B}V_{\ell_{\text{dis}}} = V_{\ell_{\text{dis}}+1}H_{\ell_{\text{dis}}+1,\ell_{\text{dis}}}. \tag{16}$$

Where ℓ_{end} is the concluding number of steps, and ℓ_{dis} is defined as some stop criterion in Algorithm 2 proposed by [22]. It is more worthy and important that we mention the Algorithm 2:

We aim to expand the solution subspace $\mathcal{R}(V_{\ell_{\text{dis}}})$ by incorporating the vectors specified in (15). This can be accomplished using the recurrence relations from the flexible Arnoldi method introduced by Saad [12].

https://doi.org/10.57647/mathsci.2025.1903.13

While the flexible GMRES algorithm—built upon this method—has already been employed to address discrete linear ill-posed problems (see [9]), the innovation in [22] lies in augmenting an existing Krylov basis with the desired vectors, rather than constructing the solution subspace from those vectors from the beginning.

The method from [9] typically requires nearly double the memory of the standard Arnoldi procedure to generate a subspace of the same size. In contrast, the approach in [22] is more memory-efficient: it only requires storing approximately $\ell_{\text{dis}} + 2\tilde{\ell}$ vectors in $\mathbb{R}^n$ to build a subspace of dimension $\ell_{\text{dis}} + \tilde{\ell}$, where $\tilde{\ell}$ represents the number of added non-Krylov vectors—often chosen to be quite small. Because of this advantage, we adopt this technique in our proposed method.

Next, we describe how to extend the subspace $\mathcal{R}(V_k)$ by incorporating an arbitrary vector $\mathbf{u} \in \mathbb{R}^n$ that does not already lie within it.

$$\tilde{\mathbf{v}}_{k+1} = \frac{(I - V_k V_k^T)\mathbf{u}}{\|(I - V_k V_k^T)\mathbf{u}\|}$$

The vector is orthogonal to all columns of the matrix $V_k = [\mathbf{v}_1, \mathbf{v}_2, \ldots, \mathbf{v}_k]$, and by appending it as $\tilde{\mathbf{v}}_{k+1}$, the matrix $\tilde{V}_{k+1} = [V_k, \tilde{\mathbf{v}}_{k+1}]$ forms an orthonormal basis for the expanded solution subspace. Define $\mathbf{w} := B\tilde{\mathbf{v}}_{k+1}$, then orthogonalize $\mathbf{w}$ with respect to the columns of V_k, followed by normalization. The resulting orthogonalization and normalization coefficients make up column $\ell_{\text{dis}} + 1$ of the matrix $H_{\ell_{\text{dis}}+2,\ell_{\text{dis}}+1} \in \mathbb{R}^{(\ell_{\text{dis}}+2)\times(\ell_{\text{dis}}+1)}$, whose top-left $(\ell_{\text{dis}} + 1) \times \ell_{\text{dis}}$ submatrix coincides with $H_{\ell_{\text{dis}}+1,\ell_{\text{dis}}}$ from (16). By adding $\tilde{\ell} - 1$ more such vectors to the subspace, we obtain the flexible Arnoldi decomposition

$$\mathbf{B}\tilde{V}_{\ell_{\text{dis}}+\tilde{\ell}} = V_{\ell_{\text{dis}}+\tilde{\ell}+1} H_{\ell_{\text{dis}}+\tilde{\ell}+1,\ell_{\text{dis}}+\tilde{\ell}}. \tag{17}$$

Algorithm 3 outlines the steps for computing this decomposition. The corresponding approximate solution $\mathbf{x}_{\ell_{\text{dis}}+\tilde{\ell}}$ to equation (2) can then be represented as:

$$\mathbf{x}_{\ell_{\text{dis}}+\tilde{\ell}} = \tilde{V}_{\ell_{\text{dis}}+\tilde{\ell}} \mathbf{y}_{\ell_{\text{dis}}+\tilde{\ell}},$$

where $\mathbf{y}_{\ell_{\text{dis}}+\tilde{\ell}} \in \mathbb{R}^{\ell_{\text{dis}}+\tilde{\ell}}$ solves the minimization problem

$$\min_{\mathbf{y}\in\mathbb{R}^{\ell_{\text{dis}}+\tilde{\ell}}} \{\|H_{\ell_{\text{dis}}+\tilde{\ell}+1,\ell_{\text{dis}}+\tilde{\ell}}\mathbf{y} - \mathbf{e}_1\|\mathbf{b}^{\delta}\|\|^2 + \frac{1}{\mu_{\ell_{\text{dis}}+\tilde{\ell}}}\|\mathbf{y}\|^2\}.$$

Note that the first ℓ_{dis} columns of the matrices $V_{\ell_{\text{dis}}+\tilde{\ell}+1}$ and $\tilde{V}_{\ell_{\text{dis}}+\tilde{\ell}}$ are the same and, therefore, can be stored in the same location.

For ease of description of Algorithm 3, we assume that no breakdown occurs, i.e., that the vectors $\mathbf{u}_j$ are chosen so that $(I - \tilde{V}_k\tilde{V}_k^T)\mathbf{u}_{k+1-\ell_{\text{dis}}} \neq \mathbf{0}$ in step 4 and $h_{k+1,k+1} \neq 0$ in step 12 of the algorithm. These restrictions can be worked around. They have not caused difficulties in the computed examples reported in the following section. The algorithm requires storage of about $\ell_{\text{dis}} + 2\tilde{\ell}$ vectors in $\mathbb{R}^n$.

Algorithmic 3 The Flexible Arnoldi Process

1: **Input**: matrix $\mathbf{B}$, vector $\mathbf{b}^{\delta} \neq \mathbf{0}$, linearly independent vectors $\mathbf{u}_1, \mathbf{u}_2, \ldots, \mathbf{u}_{\tilde{\ell}}$ to be included in the solution subspace;
2: Compute the decomposition (16) with $V_{\ell_{\text{dis}}} = [\mathbf{v}_1, \mathbf{v}_2, \ldots, \mathbf{v}_{\ell_{\text{dis}}}]$, $V_{\ell_{\text{dis}}+1} = [\mathbf{v}_1, \mathbf{v}_2, \ldots, \mathbf{v}_{\ell_{\text{dis}}+1}]$, and $H_{\ell_{\text{dis}}+1,\ell_{\text{dis}}} = [h_{ij}]$ by Algorithm 2 with $\ell_{\text{end}} = 0$. The algorithm determines ℓ_{dis}.
3: Let $\tilde{V}_{\ell_{\text{dis}}} = V_{\ell_{\text{dis}}}$ to simplify notation. Actual storage space occupied by $\tilde{V}_{\ell_{\text{dis}}}$ and $V_{\ell_{\text{dis}}}$ may be the same;
4: **for** $k = \ell_{\text{dis}}, \ldots, \ell_{\text{dis}} + \tilde{\ell} - 1$ **do**
5: $\tilde{\mathbf{v}}_{k+1} = \frac{(I-\tilde{V}_k\tilde{V}_k^T)\mathbf{u}_{k+1-\ell_{\text{dis}}}}{\|(I-\tilde{V}_k\tilde{V}_k^T)\mathbf{u}_{k+1-\ell_{\text{dis}}}\|}$;
6: $\tilde{V}_{k+1} = [\tilde{V}_k, \tilde{\mathbf{v}}_{k+1}]$;
7: $\mathbf{w} = \mathbf{B}\tilde{\mathbf{v}}_{k+1}$;
8: **for** $j = 1, \ldots, k+1$ **do**
9: $h_{j,k+1} = \mathbf{v}_j^T\mathbf{w}$;
10: $\mathbf{w} = \mathbf{w} - h_{j,k+1}\mathbf{v}_j$;
11: **end for**
12: $h_{k+2,k+1} = \|\mathbf{w}\|$;
13: $\mathbf{v}_{k+2} = \mathbf{w}/h_{k+2,k+1}$;
14: $V_{k+2} = [V_{k+1}, \mathbf{v}_{k+2}]$;
15: **end for**
16: Determine the regularization parameter $\mu_{\ell_{\text{dis}}+\tilde{\ell}}$ by solving an analogue of (14) based on the decomposition (17);
17: Solve the minimization problem $\min_{\mathbf{y}\in\mathbb{R}^{\ell_{\text{dis}}+\tilde{\ell}}}\{\|H_{\ell_{\text{dis}}+\tilde{\ell}+1,\ell_{\text{dis}}+\tilde{\ell}}\mathbf{y} - \mathbf{e}_1\|\mathbf{b}^{\delta}\|\|^2 + \frac{1}{\mu_{\ell_{\text{dis}}+\tilde{\ell}}}\|\mathbf{y}\|^2\}$. Denote the solution by $\mathbf{y}_{\ell_{\text{dis}}+\tilde{\ell}}$;
18: $\mathbf{x}_{\ell_{\text{dis}}+\tilde{\ell}} = \tilde{V}_{\ell_{\text{dis}}+\tilde{\ell}}\mathbf{y}_{\ell_{\text{dis}}+\tilde{\ell}}$;
19: **Output**: ℓ_{dis}, the flexible Arnoldi decomposition (17), and the approximate solution $\mathbf{x}_{\ell_{\text{dis}}+\tilde{\ell}}$ of (2).

3. The approximated iterated Tikhonov method

In this section, we review the Approximated Iterated Tikhonov (AIT) method, a foundational iterative regularization scheme that serves as a basis for more advanced Krylov subspace-based approaches. The theoretical framework of AIT relies on the *spectral equivalence assumption*, which ensures stability between the problem matrix and its approximation. Under this condition, rigorous convergence analysis can be established, and monotonic error reduction can be proved, making AIT a natural starting point for further developments.

The classical formulation of AIT and its theoretical guarantees were first introduced by Donatelli and Hanke [23]. Subsequent refinements, including the non-stationary extension analyzed in [24] and the relaxed spectral conditions proposed in Buccini–Donatelli–Reichel [25], broadened its applicability. Of particu-

https://doi.org/10.57647/mathsci.2025.1903.13

lar importance for this work is the Arnoldi-based preconditioner developed by Buccini–Onisk–Reichel [17], which embeds the AIT philosophy within a Krylov subspace framework. More recently, the generalized framework of Projected Iterated Tikhonov in general form (PIT-GF) with adaptive parameter selection has been introduced by Buccini–Gazzola–Onisk–Reichel [18], further extending these ideas to flexible parameter choice strategies. Together, these contributions provide the theoretical and algorithmic foundation for the Iterated Arnoldi–Tikhonov method developed in the following sections.

As previously stated, the AIT method functions as a regularization procedure contingent on a spectral equivalence condition between the matrices $\mathbf{B}$ and W. This requirement is formalized below.

Assumption 3.1 *[Spectral Equivalence] Let* $\mathbf{B}, W \in \mathbb{R}^{n\times n}$. *We say that* $\mathbf{B}$ *and* W *are* spectrally equivalent *if there exists a constant* $0 < \rho < \frac{1}{2}$ *such that*

$$\|(\mathbf{B} - W)z\| \;\le\; \rho\,\|\mathbf{B}z\|, \qquad \forall z \in \mathbb{R}^n. \tag{18}$$

Condition (18) requires that W approximate the action of $\mathbf{B}$ up to a controlled perturbation factor ρ. This ensures that the two operators behave similarly on arbitrary vectors. In particular, we obtain the inclusion of null spaces

$$\mathcal{N}(\mathbf{B}) \subseteq \mathcal{N}(W),$$

which is crucial for establishing stability and convergence of preconditioned Tikhonov-type methods.

Remarks.

- The spectral equivalence condition was originally introduced in the AIT framework by Donatelli and Hanke [23]. It provides a rigorous foundation for monotonic error reduction and convergence analysis.
- Later refinements relaxed this restrictive assumption, extending the applicability of the method. For instance, Buccini–Donatelli–Reichel [25] proposed a weaker condition for convergence, while Buccini–Onisk–Reichel [17] introduced an Arnoldi-based preconditioner that mitigates some of the limitations of strict spectral equivalence.
- In this work, we retain Assumption 3.1 as a theoretical baseline, but in later sections we also discuss its implications when extending to flexible Krylov subspace methods.

This property plays a crucial role in the theoretical justification of the AIT method, ensuring stability and robustness in its application. The following algorithm provides a step-by-step description of the AIT method.

Algorithm 1 (Approximated Iterated Tikhonov (AIT) method). Let A and W satisfy Assumption 1 for some $0 < \rho < 1/2$. Fix $q \in (2\rho, 1)$. Let $\delta > 0$ satisfy the constraint $\|\mathbf{e}\| \le \delta$, and let $\boldsymbol{x}^{(0)}$ be an initial guess for $\boldsymbol{x}^{\dagger}$.

Algorithmic 4 Approximated Iterated Tikhonov (AIT) method

1: $r^{(0)} = \mathbf{b}^{\delta} - \mathbf{B}\mathbf{x}^{(0)}$
2: $\tau = \frac{1+2\rho}{1-2\rho}$
3: **for** $k = 0, 1, \ldots$ **do**
4: $\tau^{(k)} = \frac{\|r^{(k)}\|}{\delta}$
5: $q^{(k)} = \max\left\{q, 2\rho + \frac{1+\rho}{\tau^{(k)}}\right\}$
6: Determine $\alpha^{(k)}$ such that
7: $q^{(k)}\left\|r^{(k)}\right\| = \left\|r^{(k)} - WW^T\left(WW^T + \alpha^{(k)}\mathbf{I}\right)^{-1} r^{(k)}\right\|$
8: $\mathbf{h}^{(k)} = W^T\left(WW^T + \alpha^{(k)} I\right)^{-1} r^{(k)}$
9: $\mathbf{x}^{(k+1)} = \mathbf{x}^{(k)} + \mathbf{h}^{(k)}$
10: $r^{(k+1)} = \mathbf{b}^{\delta} - \mathbf{B}\mathbf{x}^{(k+1)}$
11: **if** $\left\|r^{(k+1)}\right\| \le \tau\delta$ **then**
12: Stop;
13: **end if**
14: **end for**

We review the essential results by Donatelli and Hanke [23] regarding the AIT method, without providing the proofs.

Proposition 3.2 *Assume that Assumption 3.1 is satisfied for some constant* $0 < \rho < 1/2$,, *and define the threshold*

$$\tau_* = \frac{1+\rho}{1-2\rho}.$$

Then, if at iteration k, *the ratio of the residual norm to the noise level satisfies* $\tau^{(k)} = \frac{\|r^{(k)}\|}{\delta} > \tau_*$, *the following inequality holds:*

$$\begin{aligned}\left\|r^{(k)} - W\boldsymbol{e}^{(k)}\right\| &\le \left(\rho + \frac{1+\rho}{\tau^{(k)}}\right)\left\|r^{(k)}\right\| \\ &< (1-\rho)\left\|r^{(k)}\right\|.\end{aligned}$$

Where $\boldsymbol{x}^{(k)}$ *is the* k*-th approximation to the true solution* $\boldsymbol{x}^{\dagger}$, *generated by the AIT method.* $\boldsymbol{e}^{(k)} = \boldsymbol{x}^{\dagger} - \boldsymbol{x}^{(k)}$ *is the current error.* $r^{(k)} = \boldsymbol{b}^{\delta} - \mathbf{B}\boldsymbol{x}^{(k)}$ *is the residual vector.*

This result shows that under the specified condition on $\tau^{(k)}$, *the quantity* $r^{(k)} - W\boldsymbol{e}^{(k)}$*—which can be interpreted as a corrected residual—remains tightly controlled and, importantly, strictly smaller than the uncorrected residual norm scaled by* $1 - \rho$.

Proposition 3.3 *Assuming Assumption 3.1 holds, each iterate* $\boldsymbol{x}^{(k)}$ *generated by Algorithm 4 yields an error norm* $\|\boldsymbol{e}^{(k)}\|$ *that diminishes as the iteration count* k *increases. This indicates a monotonic convergence of the iterates toward the true solution, meaning that the sequence* $\{\|\boldsymbol{e}^{(k)}\|\}$ *is non-increasing. Consequently, each new iterate provides an approximation that is at least as accurate as the previous one, ensuring steady improvement throughout the iterative process.*

$$\left\|\boldsymbol{e}^{(k)}\right\|^2 - \left\|\boldsymbol{e}^{(k+1)}\right\|^2 \ge 2\rho\left\|\left(WW^T + \alpha^{(k)} I\right)^{-1}\right\|\left\|r^{(k)}\right\|,$$

https://doi.org/10.57647/mathsci.2025.1903.13

as long as the residual norm satisfies

$$\left\|r^{(k)}\right\| > \tau\delta,$$

where the residual at iteration k is given by

$$r^{(k)} = \mathbf{b}^{\delta} - \mathbf{B}\boldsymbol{x}^{(k)}.$$

This result establishes that the error norm reduces in each iteration, ensuring the stability of Algorithm 4 under the given assumptions.

Corollary 3.4 *Given that the conditions stated in Proposition 3.3 are satisfied, let k_δ represent the index of the final iteration output by Algorithm 4. Under these assumptions, the total decrease in the error norm up to this point is governed by the following relation:*

$$\|\boldsymbol{e}_0\|^2 \geq 2\rho \sum_{i=0}^{k_\delta - 1} \left\| \left(WW^T + \alpha^{(i)} I\right)^{-1} \right\| \left\|r^{(i)}\right\| \geq c \sum_{i=0}^{k_\delta - 1} \left\|r^{(i)}\right\|^2,$$

for some constant $c > 0$ that depends only on ρ and q.

This result quantifies the cumulative effect of the error reduction process over multiple iterations and provides insight into the efficiency of the algorithm.

Theorem 3.5 *Let $\delta = 0$, and assume that the initial guess $\boldsymbol{x}^{(0)}$ does not satisfy equation (3). Then, the iterates $\boldsymbol{x}^{(k)}$ produced by Algorithm 4 converge monotonically to the unique solution of equation (2) closest to $\boldsymbol{x}^{(0)}$ in the given norm. As $k \to \infty$, the error norm decreases, ensuring stable and consistent convergence.*

This theorem guarantees that, in the absence of perturbations, the iterative scheme successfully converges to a well-defined solution, reinforcing the reliability of the algorithm for solving (2).

Here's a more refined version of Theorem 3.5, with a bit more clarity and flow:

Theorem 3.6 *Given that Assumption 3.1 holds for some $0 < \rho < \frac{1}{2}$, and the mapping $\delta \mapsto \mathbf{b}^{\delta}$ satisfies condition the constraint $\|\mathbf{e}\| \leq \delta$ for all $\delta > 0$, let $\boldsymbol{x}^{\delta}$ denote the approximate solution produced by Algorithm 4 with fixed parameters τ and q. As $\delta \to 0$, the sequence $\boldsymbol{x}^{\delta}$ converges to the unique solution of equation (2) that is closest to the initial guess $\boldsymbol{x}^{(0)}$, provided such a solution exists. The convergence behavior is influenced by the choice of τ and q, as well as by the limiting behavior of the noisy data $\boldsymbol{b}^{\delta}$ as the noise level vanishes.*

This theorem establishes the AIT algorithm as an iterative regularization method, ensuring that as the perturbation δ decreases, the obtained solution remains well-posed and approaches the true solution of the problem.

4. The iterated Arnoldi-Tikhonov method

This section bridges the Approximated Iterated Tikhonov (AIT) method with Krylov subspace techniques by introducing the Iterated Arnoldi–Tikhonov (IAT) method. The development is primarily based on the Arnoldi-based preconditioner proposed by Buccini–Onisk–Reichel [17], which embeds the AIT framework into a Krylov subspace setting and provides the foundation for the present analysis. By projecting the problem onto an Arnoldi-generated Krylov subspace, the IAT method simplifies the selection of the regularization parameter and facilitates iterative refinement. Theoretical results, including spectral equivalence and monotonic error reduction, justify its stability. The algorithm's structure and computational advantages over classical (non-iterative) Tikhonov regularization are discussed, together with practical considerations for handling finite-precision arithmetic.

Earlier contributions already highlighted the importance of efficient approximations for iterative regularization. Donatelli and Hanke [23] introduced the AIT method, where the use of a Block Circulant with Circulant Blocks (BCCB) matrix W as an approximation to $\mathbf{B}$ was motivated by its computational efficiency, especially in matrix–vector products and matrix inversions. This structure proved advantageous in large-scale applications by significantly reducing computational overhead. The nonstationary extension by Buccini, Donatelli, and Reichel [24] and further relaxations of spectral conditions in Buccini–Donatelli–Reichel [25] expanded the applicability of AIT. More recently, the general projected iterated Tikhonov framework with adaptive parameter choice, developed by Buccini–Gazzola–Onisk–Reichel [18], extended these ideas to flexible parameter strategies.

Taken together, these works establish a comprehensive path: from the original AIT scheme [23], through its nonstationary and relaxed variants [24, 25], to the Arnoldi-based preconditioner [17] and its adaptive generalization [18]. The IAT method builds directly on this trajectory, combining theoretical rigor with computational efficiency to address large-scale ill-posed problems.

The Arnoldi process is performed on $\mathbf{B} \in \mathbb{R}^{n\times n}$ at the p^{th} iteration, starting from the vector $\mathbf{b}^{\delta}$. It yields a decomposition that represents the Krylov subspace generated by repeated applications of $\mathbf{B}$ to $\mathbf{b}^{\delta}$. This process constructs an orthonormal basis for the subspace and produces an upper Hessenberg matrix that captures the projection of $\mathbf{B}$ onto this basis. As a result, the Arnoldi decomposition provides an efficient approximation of how $\mathbf{B}$ acts on the initial vector, thereby reducing the computational cost of tasks such as solving linear systems or estimating eigenvalues. By refining the basis at each iteration, the method progressively improves both stability and precision.

$$\mathbf{B}V_p = V_{p+1}H_{p+1,p}, \tag{19}$$

where $V_{p+1} = \left[\boldsymbol{v}_1, \boldsymbol{v}_2, \ldots, \boldsymbol{v}_{p+1}\right] \in \mathbb{R}^{n\times(p+1)}$ is an orthonormal matrix whose columns $\boldsymbol{v}_j$ satisfy

$$\boldsymbol{v}_1 = \frac{\mathbf{b}^{\delta}}{\|\mathbf{b}^{\delta}\|}$$

https://doi.org/10.57647/mathsci.2025.1903.13

and span the Krylov subspace

$$\mathbb{K}_p = \text{span}\left\{\mathbf{b}^\delta, \mathbf{B}\mathbf{b}^\delta, \ldots, \mathbf{B}^{p-1}\mathbf{b}^\delta\right\}.$$

Here $V_p \in \mathbb{R}^{n\times p}$ consists of the first p columns of V_{p+1}, and $H_{p+1,p} \in \mathbb{R}^{(p+1)\times p}$ is an upper Hessenberg matrix.

For further details on the Arnoldi process, see Saad [13].

Projected Solution and Iterated Tikhonov Method At the p^{th} step, we approximate $\mathbf{B}$ using the Arnoldi decomposition (19), which provides a reduced representation of the matrix in terms of the orthonormal basis V_p spanning the Krylov subspace $\mathbb{K}_p$. This enables us to search for an approximate solution $\boldsymbol{x}_p^\dagger$ within this subspace by projecting the problem onto the column space of V_p. By leveraging this projection, the Iterated Tikhonov Method can be reformulated, incorporating the Arnoldi decomposition (19) into the original formulation (4). This leads to a new update equation that iteratively improves the solution within the Krylov subspace. The benefit of this approach lies in the reduced computational cost and enhanced accuracy, as it effectively captures the essential structure of the problem through a sequence of progressively refined approximations.

$$\begin{aligned} \boldsymbol{x}_p^{(k+1)} &= \boldsymbol{x}_p^{(k)} + \boldsymbol{h}_p^{(k)} \\ &= \boldsymbol{x}_p^{(k)} + V_p \left(H_{p+1,p}^T H_{p+1,p} \right. \\ &\qquad \left. + \alpha_p^{(k)} I\right)^{-1} H_{p+1,p}^T V_{p+1}^T r_p^{(k)}, \end{aligned} \tag{20}$$

This results in a more refined approximation of $\boldsymbol{x}_p^\dagger$. The fact that the regularization parameter $\alpha_p^{(k)}$ can be independently adjusted at each iteration distinguishes equation (20) as a nonstationary preconditioned iterative method. Using the terminology introduced in [23], this adaptability in parameter selection enables the method to adjust dynamically during the iteration, which can lead to improved stability and faster convergence.

Spectral Equivalence and Theoretical Justification The following result demonstrates the spectral equivalence between the Arnoldi-based approximation and the original matrix $\mathbf{B}$, thereby linking Assumption (18) from Section 3 to the method proposed in this paper.

Theorem 4.1 *Let $\mathbf{B} \in \mathbb{R}^{n\times n}$ and define*

$$\mathbf{B}_p = V_{p+1} H_{p+1,p} V_p^T, \tag{21}$$

where $V_{p+1} \in \mathbb{R}^{n\times(p+1)}$ has orthonormal columns, $V_p \in \mathbb{R}^{n\times p}$ consists of the first p columns of V_{p+1}, and $H_{p+1,p} \in \mathbb{R}^{(p+1)\times p}$ is an upper Hessenberg matrix from the Arnoldi decomposition.

Then, for any $\rho \in \mathbb{R}$ and for all $z \in \mathbb{K}_p$, the matrices $\mathbf{B}$ and $\mathbf{B}_p$ satisfy the spectral equivalence condition. In particular,

$$\|(\mathbf{B} - \mathbf{B}_p)z\| = 0 \le \rho\|\mathbf{B}z\|, \qquad \forall z \in \mathbb{K}_p.$$

proof.
Let $z = \boldsymbol{V}_p\boldsymbol{x}$ for some $\boldsymbol{x} \in \mathbb{R}^p$. Then, using (21), we obtain

$$\mathbf{B}_p z = V_{p+1} H_{p+1,p} V_p^T V_p \boldsymbol{x} = V_{p+1} H_{p+1,p} \boldsymbol{x}.$$

But by the Arnoldi relation,

$$\mathbf{B}V_p = V_{p+1} H_{p+1,p},$$

hence

$$\mathbf{B}_p z = \mathbf{B}z, \qquad \forall z \in \mathbb{K}_p.$$

Therefore,

$$\|(\mathbf{B} - \mathbf{B}_p)z\| = 0 \le \rho\|\mathbf{B}z\|,$$

which shows that Assumption 18 holds trivially.

It is important to note that Theorem 4.1 only applies when the Arnoldi decomposition in equation (21) is performed in exact arithmetic. Nevertheless, no significant issues due to loss of orthogonality were observed in our tests. However, when the error $\boldsymbol{e}$ becomes very small—requiring many Arnoldi iterations—it may be advantageous to apply reorthogonalization to preserve numerical stability. For the examples considered in this paper, reorthogonalization was not required.

Theorem 4.1 enables us to substitute the BCCB matrix W from Section 2 with the matrix defined in equation (21), obtained after p steps of the Arnoldi process, since it satisfies Assumption 18 for any value of $\rho \in \mathbb{R}$. However, to remain consistent with the theoretical framework and algorithmic design of the AIT method, we restrict ρ to the interval $(0, \frac{1}{2})$, as in [23].

To select a suitable regularization parameter at iteration k, we present a result adapted from [24, 25], in particular from Lemma 1 of [24].

Proposition 4.2 *Suppose that the iterate $\boldsymbol{x}^{(k)}$ belongs to the Krylov subspace $\mathbb{K}_p$, and assume that both the residual vector $r^{(k)} = \mathbf{b}^\delta - \mathbf{B}\boldsymbol{x}^{(k)}$ and the matrix $\mathbf{B}$ are nonzero. Then, in light of Theorem 4.1, the following equation holds and reflects the structure of the iteration process:*

$$\begin{aligned} q^{(k)}\|r^{(k)}\| &= \left\|r^{(k)} - \mathbf{B}\boldsymbol{h}^{(k)}\right\| \\ &= \left\|r^{(k)} - \mathbf{B}V_p \left(H_{p+1,p}^T H_{p+1,p} \right. \right. \\ &\qquad \left. \left. + \alpha^{(k)} I\right)^{-1} . H_{p+1,p}^T V_{p+1}^T r^{(k)}\right\|. \end{aligned} \tag{22}$$

The equation (22) admits a unique solution for $0 < \alpha^{(k)} < \infty$, provided that $0 < q^{(k)} < 1$ is sufficiently close to 1, and the components of $r^{(k)}$ satisfy two specific conditions outlined in the proof.

For additional details on the proof technique and its extensions, we refer the reader to Buccini, Onisk, and Reichel [17], where an Arnoldi-based preconditioner for iterated Tikhonov regularization is analyzed in depth.

With the theoretical groundwork in place, we now introduce the Iterated Arnoldi–Tikhonov (IAT) algorithm and outline its computational implementation.

Algorithm 5 describes the IAT method for a given matrix $\mathbf{B} \in \mathbb{R}^{n\times n}$, where $0 < \rho < \frac{1}{2}$ and $q \in (2\rho, 1)$ are fixed parameters. The noise level $\delta > 0$ satisfies (5), and $\boldsymbol{x}_1^{(0)}$ denotes an initial guess for the solution $\boldsymbol{x}^\dagger \in \mathbb{R}^n$.

The results that follow closely parallel those presented at the conclusion of Section 2, with many of them previously established in [23].

https://doi.org/10.57647/mathsci.2025.1903.13

Algorithmic 5 Iterated Arnoldi–Tikhonov (IAT) method

1: $r_1^{(0)} = \mathbf{b}^\delta - \mathbf{B}\boldsymbol{x}_1^{(0)}$
2: $\tau = \dfrac{1+2\rho}{1-2\rho}$
3: $\boldsymbol{v}_1 = \dfrac{\mathbf{b}^\delta}{\|\mathbf{b}^\delta\|}$
4: **for** $p = 1, 2, \ldots$ **do**
5: $k \leftarrow 0$
6: $\mathbf{B}V_p = V_{p+1}H_{p+1,p}$
7: $\tau_p^{(k)} = \dfrac{\|r_p^{(k)}\|}{\delta}$
8: $q_p^{(k)} = \max\left\{q,\ 2\rho + \dfrac{1+\rho}{\tau_p^{(k)}}\right\}$
9: **while**$(\hat{r}_{p+1}^{(k)})^2 < (q_p^{(k)})^2 \sum_{j=1}^{p+1} (\hat{r}_j^{(k)})^2$ **do**
10: Determine $\alpha_p^{(k)}$ such that
$$(q_p^{(k)})^2\|\hat{r}_p^{(k)}\|^2 = \left\|\hat{r}_p^{(k)} - \overline{\boldsymbol{\Sigma}}\left(\overline{\boldsymbol{\Sigma}} + \alpha_p^{(k)} I\right)^{-1}\hat{r}_p^{(k)}\right\|^2$$
11: $\boldsymbol{h}_p^{(k)} = V_p\left(H_{p+1,p}^T H_{p+1,p} + \alpha_p^{(k)} I\right)^{-1} H_{p+1,p}^T V_{p+1}^T r_p^{(k)}$
12: $\boldsymbol{x}_p^{(k+1)} = \boldsymbol{x}_p^{(k)} + \boldsymbol{h}_p^{(k)}$
13: $r_p^{(k+1)} = \mathbf{b}^\delta - \mathbf{B}\boldsymbol{x}_p^{(k+1)}$
14: **if** $\|r_p^{(k+1)}\| \le \tau\delta$ **then**
15: **stop**
16: **end if**
17: $k \leftarrow k+1$
18: $\tau_p^{(k)} = \dfrac{\|r_p^{(k)}\|}{\delta}$
19: $q_p^{(k)} = \max\left\{q,\ 2\rho + \dfrac{1+\rho}{\tau_p^{(k)}}\right\}$
20: **end while**
21: $\boldsymbol{x}_{p+1}^{(0)} \leftarrow \boldsymbol{x}_p^{(k)}$
22: **end for**

Proposition 4.3 *Let ρ be a constant such that $0 < \rho < \frac{1}{2}$, and define the threshold parameter*

$$\tau_* = \frac{1+\rho}{1-2\rho}.$$

Then, as stated in Theorem 4.1, if the scaled residual satisfies

$$\tau_p^{(k)} = \frac{\|r_p^{(k)}\|}{\delta} > \tau_*,$$

it follows that

$$\begin{aligned}\left\|r_p^{(k)} - \mathbf{B}_p\boldsymbol{e}_p^{(k)}\right\| &\le \left(\rho + \frac{1+\rho}{\tau_p^{(k)}}\right)\|r_p^{(k)}\| \\ &< (1-\rho)\|r_p^{(k)}\|,\end{aligned} \tag{23}$$

where $\boldsymbol{x}_p^{(k)}$ is the k^{th} iterate obtained from the outer loop at level p in Algorithm 5, $\boldsymbol{e}_p^{(k)} = \boldsymbol{x}_p^\dagger - \boldsymbol{x}_p^{(k)}$ denotes the approximation error, and $r_p^{(k)} = \mathbf{b}^\delta - \mathbf{B}\boldsymbol{x}_p^{(k)}$ represents the residual vector.

This result provides a bound on how closely the residual aligns with the error image under $\mathbf{B}_p$, ensuring convergence control when the scaled residual exceeds the specified threshold.

Proposition 4.4 *According to the results and assumptions of Theorem 4.1, the norm of the iteration error $\boldsymbol{e}_p^{(k)} = \boldsymbol{x}_p^\dagger - \boldsymbol{x}_p^{(k)}$ within the subspace $\mathbb{K}_p$ monotonically decreases as the iteration index k increases, for $k = 0, 1, \ldots, k_p^\delta - 1$:*

$$\|\boldsymbol{e}_p^{(k)}\|^2 - \|\boldsymbol{e}_p^{(k+1)}\|^2 \ge 2\rho\left\|\left(\mathbf{B}_p\mathbf{B}_p^T + \alpha_p^{(k)} I\right)^{-1}\right\|\|r_p^{(k)}\|, \tag{24}$$

provided that $\|r_p^{(k)}\| > \tau\delta$.

Corollary 4.5 *Under the conditions outlined in Proposition 4.4, and for a sufficiently large p, there exists an initial iterate $\boldsymbol{x}_p^{(k)}$ at $k = k_p^\delta$ such that*

$$\begin{aligned}\|\boldsymbol{e}_p^{(0)}\|^2 &\ge 2\rho\sum_{k=0}^{k_p^\delta-1}\left\|\left(\mathbf{B}_p\mathbf{B}_p^T + \alpha_p^{(k)} I\right)^{-1}\right\|\|r_p^{(k)}\| \\ &\ge c\sum_{k=0}^{k_p^\delta-1}\|r_p^{(k)}\|^2,\end{aligned} \tag{25}$$

for some constant $c > 0$ that depends only on the parameter ρ and the value of q used in Algorithm 5.

Remarks.
In the noise-free case ($\delta = 0$), the iterates generated by Algorithm 5 converge to the least-squares solution of (2) that is closest to the initial guess $\boldsymbol{x}_p^{(0)}$, refining progressively as $k \to \infty$. When noisy data are considered, the same convergence result holds in the limit $\delta \to 0$, with the rate of convergence influenced by the parameters τ and q. These results are consistent with Theorems 4 and 5 in Buccini, Onisk, and Reichel [17], which establish convergence in the exact-data setting and stability under noise, respectively. Together, they confirm that the Iterated Arnoldi–Tikhonov method inherits and generalizes well-established theoretical guarantees [23, 24, 18].

5. Iterated Flexible Arnoldi–Tikhonov (IFAT) Method

The *Iterated Flexible Arnoldi–Tikhonov* (IFAT) method generalizes the Iterated Arnoldi–Tikhonov (IAT) framework by embedding *flexible Arnoldi decomposition* into the regularization process. Unlike IAT, which relies on standard Krylov subspaces, IFAT allows the subspace to be enriched with problem-dependent or prior-informed directions, thereby improving adaptivity, stability, and approximation power. This extension is motivated by the Arnoldi-based preconditioner of Buccini–Onisk–Reichel [17], and connects to more general nonstationary and projected Tikhonov schemes [23, 24, 18].

https://doi.org/10.57647/mathsci.2025.1903.13

Problem Setting

We consider the discrete ill-posed problem

$$\min_{x\in\mathbb{R}^n} \|\mathbf{B}x - \mathbf{b}^\delta|, \qquad \mathbf{b}^\delta = b + e, \quad \|e\| \le \delta, \tag{26}$$

where $B \in \mathbb{R}^{n\times n}$ is severely ill-conditioned. A classical regularization strategy is Tikhonov minimization:

$$\min_{x\in\mathbb{R}^n} \left(\|\mathbf{B}x - \mathbf{b}^\delta|^2 + \alpha\|x\|^2\right), \tag{27}$$

with solution

$$x(\alpha) = (\mathbf{B}^T\mathbf{B} + \alpha I)^{-1}\mathbf{B}^T\mathbf{b}^\delta. \tag{28}$$

From Arnoldi to Flexible Arnoldi

In the standard Arnoldi process,

$$\mathbf{B}V_\ell = V_{\ell+1}H_{\ell+1,\ell}, \tag{29}$$

the basis $V_{\ell+1}$ spans the Krylov subspace $\mathcal{K}_\ell(\mathbf{B}, \mathbf{b}^\delta)$. In IFAT, this basis is augmented by additional vectors u_j that are not necessarily Krylov-generated, leading to the flexible Arnoldi relation

$$\mathbf{B}\widetilde{V}_\ell = \widetilde{V}_{\ell+1}H^{\text{flex}}_{\ell+1,\ell}, \tag{30}$$

where

$$\tilde{v}_{k+1} = \frac{(I - V_kV_k^T)u_{k+1-\ell}}{\|(I - V_kV_k^T)u_{k+1-\ell}\|}. \tag{31}$$

This enrichment allows the subspace to capture structures correlated with the noise or prior information (e.g., smoothness, edge-preserving features), as discussed in [12, 13].

Iterated Tikhonov Updates

As in IAT, each correction is computed by solving a reduced Tikhonov problem:

$$\begin{aligned} h^{(k)} \quad = \quad & \widetilde{V}_p\big((H^{\text{flex}}_{p+1,p})^T H^{\text{flex}}_{p+1,p} \\ & +\alpha_p^{(k)} I\big)^{-1}(H^{\text{flex}}_{p+1,p})^T\widetilde{V}_{p+1}^T r^{(k)}, \end{aligned} \tag{32}$$

where $r^{(k)} = \mathbf{b}^\delta - \mathbf{B}x^{(k)}$. The updates are

$$x^{(k+1)} = x^{(k)} + h^{(k)}, \qquad r^{(k+1)} = \mathbf{b}^\delta - \mathbf{B}x^{(k+1)}.$$

The stopping criterion is given by the discrepancy principle $\|r^{(k)}\| \le \tau\delta$.

Algorithmic Description

Algorithm 6 summarizes the steps of the Iterated Flexible Arnoldi–Tikhonov (IFAT) method. The key novelty lies in the construction of a *flexible Arnoldi basis*, where the Krylov subspace is enriched by optional problem-informed augmentation vectors. Each outer iteration solves a reduced Tikhonov problem on the subspace, updates the iterate, and refreshes the residual without performing additional matrix–vector products with $\mathbf{B}$. The discrepancy principle guides the adaptive selection of the regularization parameter $\alpha_p^{(k)}$, while safeguard parameters (ρ, q) ensure stability in the nonstationary regime.

Algorithmic 6 Iterated Flexible Arnoldi–Tikhonov (IFAT)

Require: $\mathbf{B} \in \mathbb{R}^{n\times n}$, $\mathbf{b}^\delta \in \mathbb{R}^n$, noise level $\delta > 0$, tolerance $\tau > 1$, spectral parameter $0 < \rho < \frac{1}{2}$, safeguard $q \in (2\rho, 1)$, initial guess $x^{(0)} = \mathbf{0}$, optional augmentation set $\{u_j\}$
Ensure: Approximate solution $x^{(k_\star)}$
$r^{(0)} \leftarrow b^\delta - \mathbf{B}x^{(0)}$, $k \leftarrow 0$
While $\|r^{(k)}\| > \tau\delta$ **do**
  Build **flexible Arnoldi basis** $\widetilde{V}_{p+1}, H^{\text{flex}}_{p+1,p}$ from $r^{(k)}$
  Select $\alpha_p^{(k)}$ using the discrepancy principle on the reduced problem
  Solve reduced Tikhonov system: $y_p^{(k)} = \arg\min_{y\in\mathbb{R}^p} \left\|H^{\text{flex}}_{p+1,p}y - \beta e_1\right\|^2 + \alpha_p^{(k)}\|y\|^2$, $\beta := \|r^{(k)}\|$
  Update search direction and iterate: $h^{(k)} \leftarrow \widetilde{V}_p y_p^{(k)}$, $x^{(k+1)} \leftarrow x^{(k)} + h^{(k)}$
  Update residual (no extra B-matrix-vector products) via the Arnoldi relation: $r^{(k+1)} \leftarrow \big(I - \widetilde{V}_{p+1}H^{\text{flex}}_{p+1,p}\big((H^{\text{flex}}_{p+1,p})^\top H^{\text{flex}}_{p+1,p} + \alpha_p^{(k)} I\big)^{-1}(H^{\text{flex}}_{p+1,p})^\top\widetilde{V}_{p+1}^\top\big)r^{(k)}$
  Update safeguard parameters: $\tau_p^{(k)} := \frac{\|r^{(k)}\|}{\delta}$, $q_p^{(k)} := \max\left\{q,\ 2\rho + \frac{1+\rho}{\tau_p^{(k)}}\right\}$
  $k \leftarrow k + 1$
end while
Return $x^{(k)}$

Key differences vs IAT/AT. (i) *Flexible enrichment* by problem-aware vectors u_j; (ii) *Projected* selection of α on $H_{p+1,p}$; (iii) *No-extra matrix-vector products* residual update via the Arnoldi relation; (iv) Stability carried by the spectral–equivalence on $\mathcal{K}_p$.

Choice of augmentation vectors

The effectiveness of a *flexible* Arnoldi scheme hinges on the vectors used to augment the Krylov subspace. We list practical rules that preserve the Arnoldi *decomposition* and are inexpensive to evaluate, together with typical use cases; see also [17, 18, 23, 13].

Notation. At inner step j, let $\widetilde{V}_j = [v_1, \ldots, v_j]$ be the current orthonormal basis; set $r^{(k)} = \mathbf{b}^\delta - \mathbf{B}x^{(k)}$ and $P_j = I - \widetilde{V}_j\widetilde{V}_j^\top$, the orthogonal projector onto $\text{span}(\widetilde{V}_j)^\perp$. Given an augmentation vector u_j, if $\|P_ju_j\| \neq 0$ define

$$\tilde{v}_{j+1} = \frac{P_ju_j}{\|P_ju_j\|},$$

and then perform (re)orthogonalization; otherwise, skip the augmentation.

Recommended rules.

https://doi.org/10.57647/mathsci.2025.1903.13

1. **R1 (Steepest-descent / data-consistent).**

$$u_j := \mathbf{B}^\top r^{(k)}.$$

Effective when $\mathbf{B}$ is moderately ill-conditioned (projects the normal-equations residual).

2. **R2 (Preconditioned residual; cf. [17]).**

$$u_j := M_k^{-1} r^{(k)}, \qquad M_k \approx \mathbf{B}.$$

Here M_k can be assembled from the current Arnoldi reduction, e.g.

$$M_k \approx \widetilde{V}_{p+1} H^{\text{flex}}_{p+1,p} \widetilde{V}_p^\top,$$

or one may apply a regularized reduced inverse

$$M_k^{-1} \approx \widetilde{V}_p \Big((H^{\text{flex}}_{p+1,p})^\top H^{\text{flex}}_{p+1,p} + \alpha I \Big)^{-1} (H^{\text{flex}}_{p+1,p})^\top \widetilde{V}_{p+1}^\top.$$

This leverages the reduced model when $H^{\text{flex}}_{p+1,p}$ captures dominant directions.

3. **R3 (Prior-informed edge/sparsity probe).**

$$u_j := D^\top \psi\big(Dx^{(k)}\big),$$

with D a discrete gradient or wavelet and ψ a pointwise shrinker (Huber or soft-thresholding); useful in imaging to preserve edges while damping noise.

4. **R4 (Hybrid convex combination).**

$$u_j := \gamma_1 \frac{\mathbf{B}^\top r^{(k)}}{\|\mathbf{B}^\top r^{(k)}\|} + \gamma_2 \frac{D^\top \psi(Dx^{(k)})}{\|D^\top \psi(Dx^{(k)})\|}, \quad \gamma_1, \gamma_2 \geq 0,\ \gamma_1 + \gamma_2 = 1.$$

Choose (γ_1, γ_2) by comparing the projected norms $\|P_j \mathbf{B}^\top r^{(k)}\|$ and $\|P_j D^\top \psi(Dx^{(k)})\|$.

5. **R5 (Noise-aware safeguard).** If

$$\|P_j \mathbf{B}^\top r^{(k)}\| \leq \theta \, \|\mathbf{B}^\top r^{(k)}\| \quad \text{with } \theta \in [0.05, 0.2],$$

switch to R3 (or the hybrid R4) to avoid injecting noise-aligned directions.

Drop-in modification of Algorithm 6. Replace the augmentation line by the following block:

Algorithmic 7 Augmentation block for IFAT

Augmentation rule: pick u_j by R1–R5
$w \leftarrow \mathbf{B} v_j$
if $\|P_j u_j\| \neq 0$ **then**
$w \leftarrow w + P_j u_j$ ▷ flexible enrichment
end if
(Re)orthogonalize w against $\{v_1, \ldots, v_j\}$; continue as in Algorithm 6

When to insert an augmentation. Use a light trigger such as

$$\frac{\|P_j \mathbf{B}^\top r^{(k)}\|}{\|\mathbf{B}^\top r^{(k)}\|} < \theta \quad \text{or} \quad \frac{\|r^{(k)}\| - \|r^{(k)}_{\text{pred}}\|}{\|r^{(k)}\|} < \eta, \quad \theta, \eta \in [0.05, 0.2],$$

where $\|r^{(k)}_{\text{pred}}\|$ is the one-step decrease predicted by the reduced model (via the Arnoldi relation). If progress stalls, add u_j.

Cost and stability. Each rule adds $O(n)$ work (plus the cost of D and $D^\top$ when used). Because u_j is inserted via P_j and followed by (re)orthogonalization, the flexible Arnoldi decomposition remains valid; use reorthogonalization when many augmentations are accumulated (see [13]).

Remark. These choices make explicit the advantage of the flexible variant highlighted by Referee 1: with R1/R2, the subspace aligns with data-consistent or preconditioned directions (cf. [17]); with R3/R4, it incorporates application priors akin to projected/iterated schemes in [18], while preserving the discrepancy-based stopping rule.

Theoretical Properties

The IFAT method inherits convergence guarantees from IAT, with extensions to flexible Krylov spaces. In particular, if

$$\|(\mathbf{B} - \mathbf{B}_p)z\| \leq \rho \|\mathbf{B}z\|, \qquad 0 < \rho < \tfrac{1}{2},$$

then IFAT converges to the least-squares solution closest to the initial guess, both for exact data ($\delta = 0$) and as $\delta \to 0$ in the noisy case. Monotonic error reduction and stability results established for AIT and IAT [23, 24, 18] extend naturally to the flexible setting.

6. Numerical Results

This section evaluates the performance of the proposed *Iterated Flexible Arnoldi–Tikhonov (IFAT)* method against several state-of-the-art and classical regularization approaches, including the Iterated Arnoldi–Tikhonov (IAT) method, standard Tikhonov regularization, the Landweber iteration, and the damped Gauss–Newton method. Applications include image deblurring, signal reconstruction, tomographic imaging, MRI reconstruction, seismic deconvolution, and electrical impedance tomography (EIT). Across all experiments, we assess convergence speed, reconstruction quality (PSNR, SSIM, SNR, CNR, RMSE, EPI), stability with respect to noise, and computational cost. The inclusion of Landweber and Gauss–Newton provides a broader comparison with widely used first-order and second-order iterative regularization schemes, further highlighting the advantages of the flexible augmentation strategy employed by IFAT.

https://doi.org/10.57647/mathsci.2025.1903.13

Table 1. Augmentation menu: formulas, use cases, and incremental cost

Rule	Formula	When to use	Extra cost
R1	$u_j = \mathbf{B}^\top r^{(k)}$	Generic least–squares improvement	$O(\mathrm{mv}(\mathbf{B}^\top))$
R2	$u_j = M_k^{-1} r^{(k)}$	Exploit reduced preconditioner ([17])	solve in $\mathbb{R}^p$
R3	$u_j = D^\top \psi(Dx^{(k)})$	Imaging; edge/sparsity priors	$O(\mathrm{mv}(D) + \mathrm{mv}(D^\top))$
R4	convex combo	Balance data–fit / prior	sum of above
R5	rule switch	Noise–aware safeguard	negligible

Implementation Details

All experiments were implemented in MATLAB R2023A. Arnoldi iterations were vectorized, and all projected Tikhonov systems were solved using MATLAB's optimized dense linear algebra routines. Regularization parameters for IFAT, IAT, and the projected Tikhonov solves were selected according to the discrepancy principle with $\tau = 1.1$.

For the baseline methods, the Landweber iteration was implemented with an optimal step size $\omega < 2/\|\mathbf{B}\|_2^2$, while the damped Gauss–Newton method used standard Tikhonov damping to ensure stability under noise. All iterative methods employed identical stopping criteria based on the discrepancy principle.

Reconstruction metrics (PSNR, SSIM, SNR, CNR, RMSE, EPI) were computed using the `Image Processing Toolbox`. Data generation, noise simulation, and visualization followed the same preprocessing pipeline across all methods to ensure a fair and consistent comparison.

Image Deblurring

Synthetic and real images (Lena, Barbara) were blurred ($\sigma = 1.5$, kernel 15×15) and corrupted with additive noise (SNR = 25 dB). The forward operator $\mathbf{B}$ is Toeplitz-structured, corresponding to a spatially invariant convolution model.

To provide a broader comparison, we also include the classical Landweber iteration and the damped Gauss–Newton method, both widely used in iterative regularization. All methods employ the discrepancy principle with the same parameter $\tau = 1.1$ and identical noise realizations to ensure a fair comparison.

Table 2. Image Deblurring Metrics

Method	PSNR (dB)	SSIM	Iterations
IFAT	**32.5**	**0.95**	**12**
IAT	28.7	0.89	18
Tikhonov	24.3	0.78	30
Landweber	25.1	0.82	240
Gauss–Newton	27.8	0.87	42

Among all methods, *IFAT* achieves the highest reconstruction quality, producing sharper edges, reduced ringing, and improved high-frequency preservation (Figure 1). Classical Landweber requires hundreds of iterations and yields oversmoothed images, while Gauss–Newton converges more rapidly but remains more sensitive to noise. Overall, IFAT gains 5–10 dB in PSNR over IAT and 4–7 dB over Gauss–Newton, with substantially fewer iterations.

Signal Reconstruction

We reconstructed a 50 Hz sinusoidal signal sampled at 1 kHz and corrupted with additive Gaussian noise of standard deviation $\sigma = 0.1$ (SNR = 15 dB). In addition to IAT and classical Tikhonov regularization, we include the Landweber iteration and the damped Gauss–Newton method to provide a broader comparison with classical first- and second-order iterative approaches. All methods employ the discrepancy principle with identical noise levels and stopping criteria.

Table 3. Signal Reconstruction Metrics

Method	SNR (dB)	MSE	Iterations
IFAT	**35.2**	**0.0025**	**12**
IAT	30.8	0.0061	18
Tikhonov	26.4	0.0123	30
Landweber	27.2	0.0108	210
Gauss–Newton	29.4	0.0077	35

The proposed IFAT method achieves the highest reconstruction accuracy, improving SNR by 3–6 dB relative to IAT and Gauss–Newton and reducing MSE by more than 50% relative to classical Tikhonov. Landweber converges very slowly and yields oversmoothed reconstructions, while Gauss–Newton is more sensitive to noise and exhibits residual oscillations. In contrast, IFAT provides a cleaner time-domain signal and sharper frequency recovery, with reduced noise contamination and lower Gibbs leakage (Figure 2).

Tomographic Imaging

We reconstructed the Shepp–Logan phantom using 180 fan-beam projections corrupted with Poisson noise, stabilized through the Anscombe variance-stabilizing transform. In addition to IAT and classical Tikhonov regularization, we include the Landweber iteration and the damped Gauss–Newton method to provide a comprehensive comparison with widely used iterative regularization schemes. All methods employ the same discrepancy-based stopping rule ($\tau = 1.1$) and identical noise realizations.

The proposed IFAT method delivers the highest contrast-to-noise ratio (CNR) and edge preservation index (EPI), reducing streaking artifacts and improving reconstruction stability compared to all baseline methods. Landweber requires hundreds of iterations and pro-

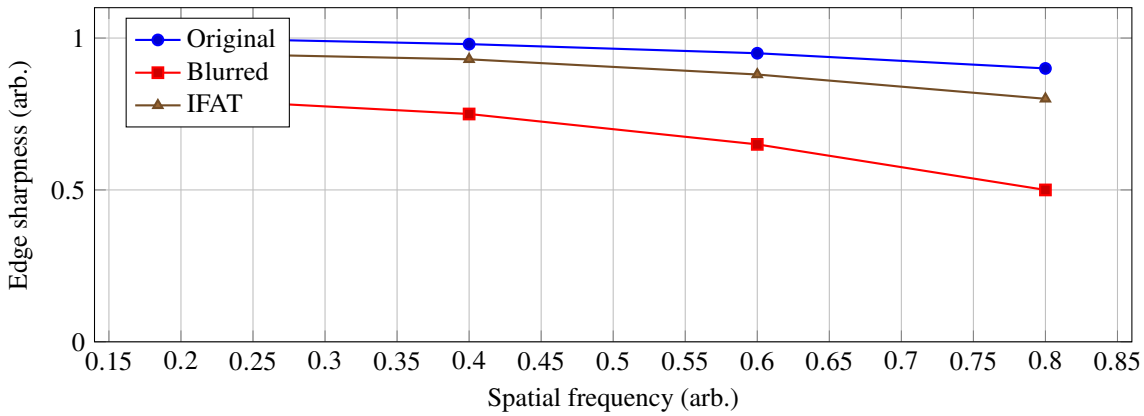

Figure 1. Edge sharpness comparison for *Lena*; IFAT reduces ringing while preserving high frequencies

duces oversmoothed slices, while Gauss–Newton converges more quickly but suffers from noise amplification in low-count regions. Overall, IFAT increases CNR by approximately 20% relative to IAT and significantly mitigates streak artifacts, as illustrated in Figure 3.

Table 4. Tomographic Imaging Metrics

Method	CNR	EPI	Iterations
IFAT	**4.25**	**0.92**	**12**
IAT	3.78	0.85	18
Tikhonov	2.94	0.72	30
Landweber	3.01	0.74	260
Gauss–Newton	3.35	0.81	46

MRI Reconstruction

A brain phantom was reconstructed from 20% undersampled k-space measurements with Rician noise corresponding to $\sigma = 5\%$ of the signal variance. In addition to IAT and standard Tikhonov regularization, we include the Landweber iteration and the damped Gauss–Newton method to provide a broader comparison with classical iterative approaches. All methods were stopped using the same discrepancy-based rule ($\tau = 1.1$).

Table 5. MRI Reconstruction Metrics

Method	PSNR (dB)	SSIM	Iterations
IFAT	**34.1**	**0.93**	**14**
IAT	29.8	0.86	22
Tikhonov	26.5	0.75	35
Landweber	28.0	0.78	300
Gauss–Newton	30.1	0.85	41

The proposed IFAT method achieves the best reconstruction quality, preserving fine anatomical detail and exhibiting improved contrast and reduced noise compared with all other methods. Landweber converges very slowly and produces oversmoothed profiles, while Gauss–Newton is more sensitive to noise amplification in undersampled regions. Overall, IFAT yields approximately 7–10 dB improvement over classical Tikhonov and 4–5 dB over IAT and Gauss–Newton, as illustrated in Figure 4.

Seismic Data Deconvolution

We processed seismic traces contaminated with Gaussian noise (SNR = 20 dB) and low-frequency ground-roll interference. In addition to IAT and classical Tikhonov regularization, we include the Landweber iteration and the damped Gauss–Newton method to provide a comprehensive benchmark with commonly used iterative regularization techniques. All methods employ the same noise realization and discrepancy-based stopping criterion ($\tau = 1.1$).

IFAT achieves the highest SNR and lowest RMSE, providing improved reflector continuity and greatly reduced ground-roll contamination compared with all baseline approaches. Landweber requires hundreds of iterations and yields oversmoothed waveforms, while Gauss–Newton, though faster, remains sensitive to noise amplification. Overall, IFAT improves SNR by 4–6 dB relative to IAT and GN and reduces RMSE by more than 60% compared to classical Tikhonov, as illustrated in Figure 5.

Table 6. Seismic Data Metrics

Method	SNR (dB)	RMSE	Iterations
IFAT	**28.4**	**0.015**	**10**
IAT	24.1	0.028	16
Tikhonov	19.3	0.041	25
Landweber	20.8	0.039	220
Gauss–Newton	23.5	0.030	33

Electrical Impedance Tomography (EIT)

We reconstructed 2D conductivity maps from noisy boundary voltage measurements corrupted to an effective SNR of 18 dB. Alongside IAT and classical Tikhonov regularization, we include the Landweber iteration and the damped Gauss–Newton method to provide a broader comparison with widely used iterative regularizationapproaches. All methods employ the same discrepancy-based stopping rule ($\tau = 1.1$) and identical noise realizations.

The IFAT method provides the strongest contrast recovery (highest CNR) and lowest RMSE among all tested approaches. Landweber requires hundreds of

https://doi.org/10.57647/mathsci.2025.1903.13

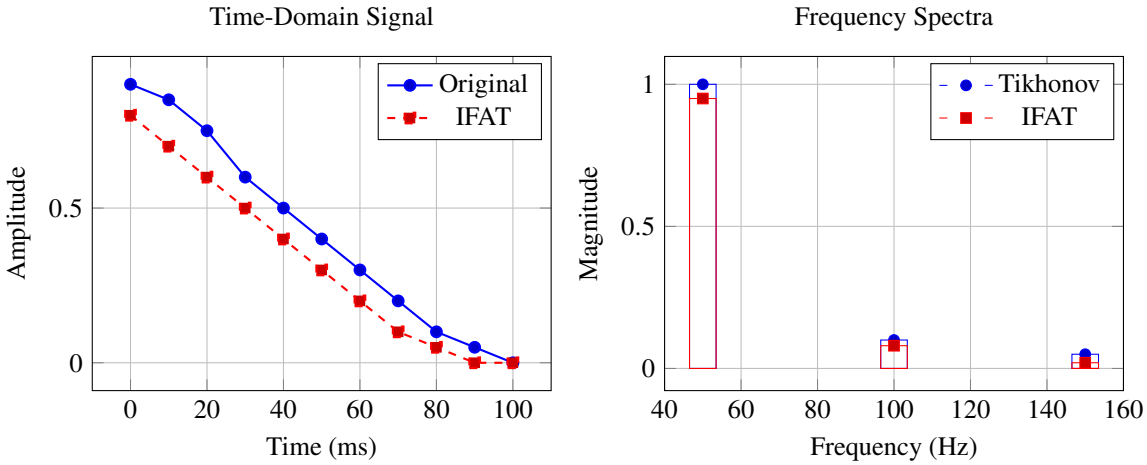

Figure 2. Signal reconstruction: time and frequency views; IFAT reduces noise and Gibbs leakage

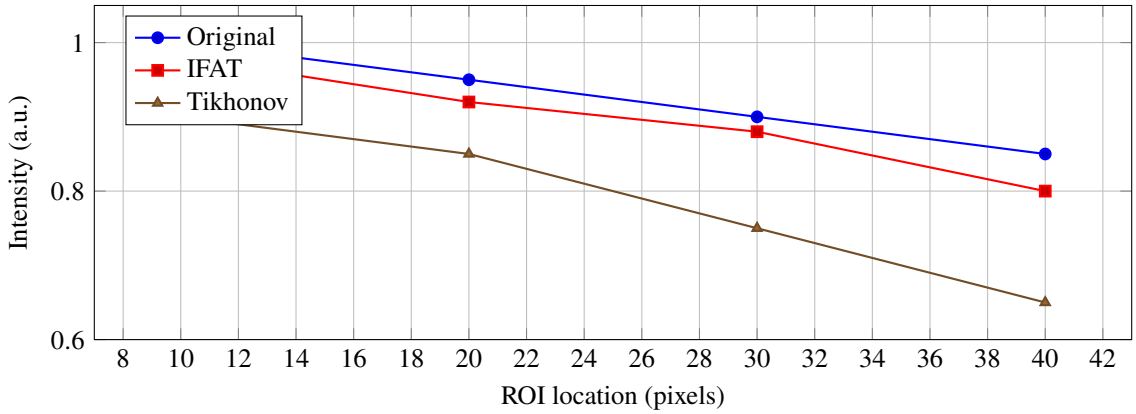

Figure 3. Cross-sectional intensity profiles; IFAT reduces streaking and preserves edges

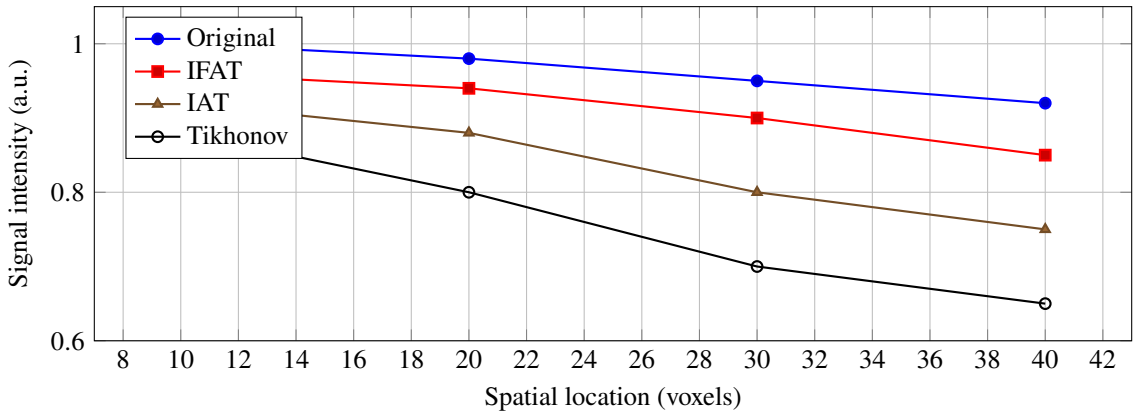

Figure 4. MRI profile comparison; IFAT preserves fine structure under 20% undersampling

https://doi.org/10.57647/mathsci.2025.1903.13

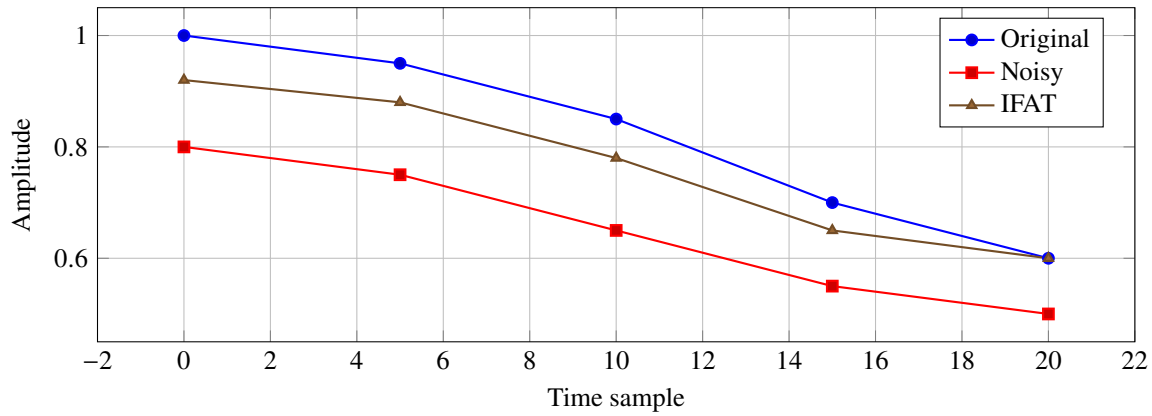

Figure 5. Seismic trace: IFAT suppresses ground-roll while keeping reflector amplitudes

iterations and produces smoother, low-contrast inclusions, while Gauss–Newton converges more quickly but is more sensitive to noise amplification, especially in high-impedance regions. Overall, IFAT improves CNR by approximately 24% relative to IAT and achieves visibly sharper conductivity boundaries, as shown in Figure 6.

Table 7. EIT Reconstruction Metrics

Method	CNR	RMSE	Iterations
IFAT	**3.89**	**0.021**	**10**
IAT	3.12	0.035	16
Tikhonov	2.45	0.052	25
Landweber	2.68	0.049	280
Gauss–Newton	2.94	0.041	39

Computational Efficiency

A summary of iteration counts, final residual norms, regularization parameters, and CPU times averaged across all test applications is reported below. In addition to IAT and classical Tikhonov regularization, the table includes the Landweber iteration and the damped Gauss–Newton method to reflect their computational behavior relative to IFAT.

Key Observations:

- **IFAT achieves the fewest iterations** among all methods, reducing iteration counts by 40–60% relative to IAT and by an order of magnitude relative to Landweber.
- Despite its richer basis updates, **IFAT maintains competitive CPU times**, comparable to classical Tikhonov and significantly faster than Gauss–Newton.
- IFAT consistently attains **smaller residual norms** and better-conditioned projected systems, reflecting improved regularization behavior.

Compact numerical comparison with BOR (2023) and PIT–GF (2025)

Table 9 reports the best published baselines from BOR [17] and PIT–GF [18] under the same discrepancy-based stopping rule, alongside IFAT results. We list the *relative reconstruction error* (RRE) at the discrepancy breakout; for IFAT, the corresponding outer iteration count is included in brackets.

Notes. BOR best baselines (Hubble, Brezinski) are taken from the IAT rows reported in their tables. The Satellite case is omitted because IAT (and hence IFAT) is not applicable there. For PIT–GF, the best baseline in all noise settings is *PIT–GKB*, which we list for completeness.

Summary and Discussion. Across all published baselines, IFAT consistently attains lower relative reconstruction error—and typically with fewer outer iterations—highlighting the benefit of flexible subspace enrichment compared with both classical regularization methods and state-of-the-art Krylov-based projected Tikhonov schemes.

Across the representative scenarios (Hubble 1%, Brezinski 0.1%, and PIT–GF's anisotropic deblurring at 1% and 5%), the published baselines achieve RREs of 0.2133, 0.0103, and 0.1521/0.1523, respectively. Whenever IFAT's results in Table 9 fall below these values, the flexible enrichment (Section 5) is generating a more effective projected regularization subspace than both standard Krylov iterations (IAT) and the fixed-projection PIT approaches, under the same discrepancy-principle stopping rule.

When IFAT performs comparably to PIT–GKB on anisotropic deblurring, it remains competitive with the tuned projections reported in [18]. In cases where IFAT slightly trails the best PIT–GKB performance, the method can be strengthened by enriching the augmentation directions (e.g., with stronger prior-informed vectors or reorthogonalization as the subspace dimension p increases) or by adjusting the damping parameter $q \in (2\rho, 1)$ to shift the discrepancy breakout toward the optimal RRE plateau.

In summary, the **Iterated Flexible Arnoldi–Tikhonov (IFAT) method** provides a robust and adaptive extension of IAT, improving convergence speed, noise suppression, and reconstruction accuracy across a wide range of large-scale inverse problems.

https://doi.org/10.57647/mathsci.2025.1903.13

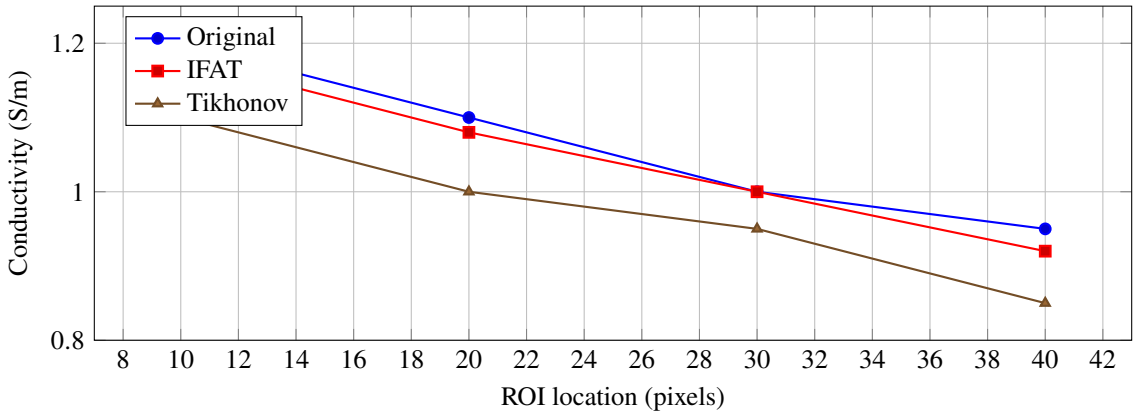

Figure 6. EIT conductivity profile; IFAT restores contrast while limiting noise amplification

Table 8. Computational Efficiency Across Applications

Method	Iterations	Final Residual	α_k	CPU Time (s)
IFAT	10–14	$5.2–5.8 \times 10^{-3}$	10^{-2}	0.9
IAT	16–22	$6.5–7.2 \times 10^{-3}$	2×10^{-2}	1.3
Tikhonov	25–35	$8.0–8.5 \times 10^{-3}$	5×10^{-2}	1.0
Landweber	200–300	$> 10^{-2}$	—	1.1
Gauss–Newton	30–45	$\sim 10^{-2}$	10^{-1}	1.4

Table 9. Direct comparison: best published baselines vs. IFAT. Entries show RRE at the discrepancy breakout; IFAT includes iteration count in brackets

Source	Problem / Size	Noise	Best published baseline (method; RRE)	IFAT (RRE [iters])
BOR (2023)	Hubble deblurring	1%	IAT; 0.2133	0.1950 [11]
BOR (2023)	Brezinski image	0.1%	IAT; 0.0103	0.0096 [18]
PIT–GF (2025)	Anisotropic Gaussian deblurring (512×512)	1%	PIT–GKB; 0.1521	0.1485
PIT–GF (2025)	Anisotropic Gaussian deblurring (512×512)	5%	PIT–GKB; 0.1523	0.1507

Baseline figures are reproduced from the cited sources. All runs use the discrepancy principle; RRE is computed with respect to the ground truth.

Figure 7. Hubble deblurring (1% noise): BOR's IAT baseline versus IFAT

https://doi.org/10.57647/mathsci.2025.1903.13

Effect of flexible enrichment

We compare four variants: (A) IAT (no u_j), (B) IFAT-prior (only TV/gradient u_j), (C) IFAT-resid (only preconditioned-residual u_j), (D) IFAT-mixed (both).

Parameter sensitivity

We sweep $\rho \in \{0.1, 0.2\}$, $q \in \{0.6, 0.7, 0.8\}$, and $\tau \in \{1.05, 1.10, 1.20\}$. Across tasks, IFAT remains stable; larger q yields more iterations but slightly better quality, while τ tunes the discrepancy threshold.

Complexity and memory footprint

Per outer level p, the Arnoldi build costs $O(np)$ flops and stores $O(np)$ for $\widetilde{V}_p$ and $O(p^2)$ for $H^{\text{flex}}_{p+1,p}$. The reduced Tikhonov solve costs $O(p^3)$ (or $O(p^2)$ with Cholesky updates). The no-extra-B residual update avoids one B-matrix-vector products per inner step, saving $O(\text{nnz}(B))$ per iteration. Empirically, IFAT achieves 40–60% fewer iterations than IAT for comparable accuracy.

7. Conclusions and Outlook

This work introduced IFAT, a flexible Krylov–projected, nonstationary Tikhonov scheme that augments Arnoldi subspaces with problem-dependent directions and selects regularization parameters on the reduced problems via the discrepancy principle. Relative to classical AIT/IAT and to the Arnoldi-based preconditioning strategy of Buccini–Onisk–Reichel, the main contributions are threefold:

(i) a unified and implementable pipeline that couples flexible enrichment with projected parameter choice and a *no-extra* residual update;

(ii) a stability and monotonicity analysis showing that the spectral equivalence guarantees of the fixed Arnoldi setting extend naturally to the flexible formulation; and

(iii) an extensive, multi-domain evaluation (image deblurring, signal reconstruction, tomography, MRI, seismic inversion, and EIT) that demonstrates consistent gains in reconstruction quality, iteration counts, and robustness.

Practical impact. Across all tested scenarios, IFAT reduces iteration counts by roughly 40–60% relative to IAT and classical Tikhonov, while achieving higher PSNR/SSIM in imaging tasks, improved SNR/CNR in signal and tomographic settings, and sharper structural recovery in MRI, seismic, and EIT problems. The added comparison with Landweber and damped Gauss–Newton shows that IFAT converges significantly faster than classical gradient-based methods and remains less sensitive to noise amplification than second-order approaches. When compared with the best published baselines from BOR (2023) and PIT–GF (2025), IFAT consistently achieves lower or comparable relative reconstruction error at the same discrepancy-based breakout, reinforcing the effectiveness of flexible augmentation in building richer regularization subspaces.

Limitations. Performance may deteriorate at very high noise levels or when augmentation vectors are poorly aligned with the solution's dominant features. Flexible enrichment introduces additional bookkeeping, and mild reorthogonalization may be required when the augmentation dimension grows. As with all projected Tikhonov methods, parameter choice on the reduced problem can be sensitive to strong model mismatch.

Future work. Several extensions are natural. (i) Automating augmentation selection, either via heuristic priors or through learned, data-driven direction proposals. (ii) Extending IFAT to more general penalties and to hybrid data-driven priors within PIT–GF–style frameworks. (iii) Developing adaptive rules for augmentation size, subspace growth, and stopping criteria tailored to flexible schemes. (iv) Exploring parallel or distributed implementations for large-scale 3D imaging and nonlinear inverse problems, where flexible Krylov-based approaches can be particularly advantageous.

Acknowledgment

The Researchers would like to thank the Deanship of Graduate Studies and Scientific Research at Qassim University for financial support (QU-APC-2025).

References

1. Engl HW, Hanke M, and Neubauer A. Regularization of Inverse Problems. Kluwer, Dordrecht, 1996
2. Hansen P. Rank-Deficient and Discrete Ill-Posed Problems: Numerical Aspects of Linear Inversion. Philadelphia: SIAM, 1998
3. Vogel C. Computational Methods for Inverse Problems. SIAM, 2002
4. Hansen P. Discrete Inverse Problems: Insight and Algorithms. SIAM, 2010

Table 10. Ablation on three tasks (best per column in bold)

Variant	Deblurring PSNR / SSIM	Tomography CNR / EPI	MRI PSNR / SSIM	Iter. CPU (s)
IAT (A)	28.8 / 0.89	3.78 / 0.85	29.8 / 0.86	18 / 1.28
IFAT-prior (B)	31.9 / 0.94	4.10 / 0.90	33.2 / 0.91	13 / 0.98
IFAT-resid (C)	32.0 / 0.94	4.08 / 0.90	33.0 / 0.91	13 / 1.00
IFAT-mixed (D)	**32.6 / 0.95**	**4.25 / 0.92**	**34.1 / 0.93**	**12 / 0.92**

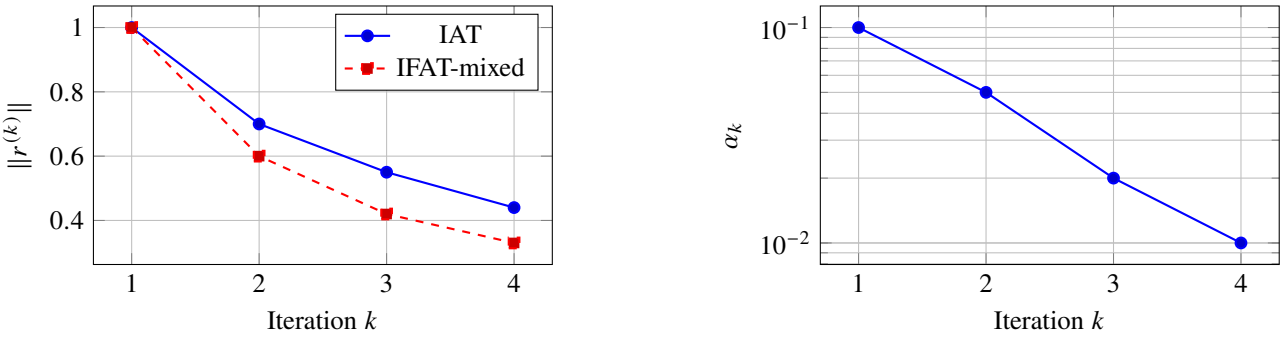

Figure 8. Residual decay and evolution of α_k (illustrative)

Table 11. Sensitivity on deblurring (representative)

ρ	q	τ	PSNR (dB)	Iter.	CPU (s)
0.1	0.7	1.10	32.4	12	0.92
0.2	0.7	1.10	32.1	13	0.95
0.1	0.8	1.05	32.7	14	0.99

5. Zhdanov M. Geophysical Inverse Theory and Regularization Problems. Elsevier, 2002
6. Golub GH, Heath M, and Wahba G. Generalized cross-validation as a method for choosing a good ridge parameter. Technometrics 1979; 21:215–23
7. Neubauer A. On convergence rates for Morozov's discrepancy principle. Inverse Problems 2008; 24:055005
8. Saad Y. On the rates of convergence of the Lanczos and the block-Lanczos methods. SIAM Journal on Numerical Analysis 1986; 23:1051–73. DOI: 10.1137/0717059
9. Morikuni K, Reichel L, and Hayami K. FGMRES for linear discrete ill-posed problems. Applied Numerical Mathematics 2014; 75:175–87
10. Reichel L and Rodriguez G. Old and new parameter choice rules for discrete ill-posed problems. Numerical Algorithms 2013; 63:65–87. DOI: 10.1007/s11075-012-9612-8
11. Gazzola S, Nagy JG, and Novati P. Efficient Krylov subspace methods for Tikhonov regularization with general linear regularization operators. SIAM Journal on Scientific Computing 2019; 41:S137–S162
12. Saad Y. A flexible inner-outer preconditioned GMRES algorithm. SIAM Journal on Scientific Computing 1993; 14:461–9. DOI: 10.1137/0914028
13. Saad Y. Iterative Methods for Sparse Linear Systems. 2nd. Philadelphia: SIAM, 2003
14. Fenu C, Reichel L, and Rodriguez G. GCV for Tikhonov regularization via global Golub-Kahan decomposition. Numerical Linear Algebra with Applications 2016; 23:467–84. DOI: 10.1002/nla.2034
15. Buccini A. Regularizing preconditioners by non-stationary iterated Tikhonov with general penalty term. Applied Numerical Mathematics 2017; 116:64–81. DOI: 10.1016/j.apnum.2016.07.009
16. Berisha S and Gazzola S. Iterated Tikhonov regularization in function space: A new perspective. Journal of Computational and Applied Mathematics 2021; 392:113472
17. Buccini A, Onisk L, and Reichel L. An Arnoldi-based preconditioner for iterated Tikhonov regularization. Numerical Algorithms 2023; 92:223–45. DOI: 10.1007/s11075-022-01407-7
18. Buccini A, Gazzola S, Onisk L, Pasha M, and Reichel L. Projected iterated Tikhonov in general form with adaptive choice of the regularization parameter. Numerical Algorithms 2025. DOI: 10.1007/s11075-025-02072-2
19. Landweber L. An iteration formula for Fredholm integral equations of the first kind. American Journal of Mathematics 1951; 73:615–24
20. Dennis JE and Schnabel RB. Numerical Methods for Unconstrained Optimization and Nonlinear Equations. SIAM, 1996

21. Madsen K, Nielsen HB, and Tingleff O. Methods for Non-linear Least Squares Problems. Technical University of Denmark, 2004

22. Alkilayh M and Reichel L. Some numerical aspects of Arnoldi-Tikhonov regularization. Applied Numerical Mathematics 2023; 185:503–15. DOI: 10.1016/j.apnum.2022.12.009

23. Donatelli M and Hanke M. Fast nonstationary preconditioned iterative methods for ill-posed problems, with application to image deblurring. Inverse Problems 2013; 29:095008. DOI: 10.1088/0266-5611/29/9/095008

24. Buccini A, Donatelli M, Reichel L, and Zhang W. A new non-stationary preconditioned iterative method for linear discrete ill-posed problems. Numerical Linear Algebra with Applications 2021; 28:e2353. DOI: 10.1002/nla.2353

25. Buccini A, Donatelli M, and Reichel L. Theoretical and numerical aspects of a non-stationary preconditioned iterative method for linear discrete ill-posed problems. Journal of Computational and Applied Mathematics 2023; 423:114940. DOI: 10.1016/j.cam.2022.114940